O'Shea, D. G., Ward, J. M., Shortt, B. J., Mortier, M., Féron, P., Nic Chormaic, S., 2007. Upconversion channels in Er^{3+}:ZBLALiP fluoride glass microspheres. *European Physical Journal Applied Physics*, 40(2), pp.181-188. DOI: 10.1051/epjap:2007148

Eur. Phys. J. Appl. Phys. **40**, 181–188 (2007)
DOI: 10.1051/epjap:2007148

THE EUROPEAN PHYSICAL JOURNAL APPLIED PHYSICS

Upconversion channels in Er^{3+}:ZBLALiP fluoride glass microspheres

D.G. O'Shea[1,2], J.M. Ward[2,3], B.J. Shortt[2,3], M. Mortier[4], P. Féron[5], and S. Nic Chormaic[1,2,a]

[1] Physics Department, University College Cork, Cork, Ireland
[2] Photonics Centre, Tyndall National Institute, Prospect Row, Cork, Ireland
[3] Department of Applied Physics and Instrumentation, Cork Institute of Technology, Bishopstown, Cork, Ireland
[4] Laboratoire de Chimie de la Matière Condensée de Paris, ENSCP, 11 rue Pierre et Marie Curie, 75005 Paris, France
[5] ENSSAT-FOTON (CNRS-UMR 6082) Université de Rennes 1, 6 rue de Kerampont, BP 80518, 22305 Lannion Cedex, France

Received: 29 May 2007 / Received in final form: 21 August 2007 / Accepted: 28 August 2007
Published online: 31 October 2007 –

Abstract. We present results on the realization of a multicolour microspherical glass light source fabricated from the erbium doped fluoride glass ZBLALiP. Whispering gallery mode lasing and upconversion processes give rise to laser and fluorescent emissions at multiple wavelengths from the ultraviolet to the infrared. Thirteen discrete emissions ranging from 320 to 849 nm have been observed in the upconversion spectrum. A Judd-Ofelt analysis was performed to calculate the radiative properties of Er^{3+}:ZBLALiP microspheres, including the radiative transition probabilities, the electric dipole strengths, the branching ratios and the radiative lifetimes of the transitions involved. We have also identified the primary processes responsible for the generation of the observed wavelengths and have shown that this material has an improved range of emissions over other erbium doped fluoride glasses.

PACS. 42.55.Sa Microcavity and microdisk lasers – 42.70.Hj Laser materials – 42.70.Ce Glasses, quartz

1 Introduction

Microspherical resonators have attracted significant attention in recent years due to their interesting optical properties and the range of applications for which they can be used including quantum optics [1–3] and optical communications [4,5]. In particular, microspheres fabricated from rare-earth ion doped materials have been shown to operate as miniature laser devices [6,7]. Recently, there have been significant breakthroughs in the exploitation of upconversion mechanisms in rare-earth ion doped materials to yield wavelengths from the near infrared to the near ultraviolet. The spectral properties of the emissions from the materials depend on (i) the choice of dopant (e.g. Er^{3+}, Yb^{3+}) and (ii) the host matrix (e.g. fluoride or phosphate glass) in which the dopant is embedded. The close proximity of numerous energy levels in triply-ionized rare earth ions is advantageous for obtaining fluorescent and lasing emissions through various upconversion mechanisms such as excited state absorption (ESA), energy transfer upconversion (ETU) and photon avalanche (PA) [8].

Three-photon upconversion lasing yielding red and blue emissions about 480 nm and 800 nm in thulium-doped fluorozirconate (ZBLAN) glass microspheres has been reported [9]. The same authors also observed red and green upconversion lasing in erbium doped ZBLAN glass microspheres [10]. In both cases, 1064 nm free-space laser pulses focused on the microsphere surface acted as the pump source. The first microspherical laser pumped using a fibre taper was demonstrated when an Yb:Er-doped phosphate glass microsphere was pumped at 980 nm [11]. The microsphere lased in the infrared about 1550 nm with a threshold power of 60 μW, and emitted green fluorescence attributed to a two-photon ESA process. Several groups [6,7,12,13] have also made considerable progress in the development of microspherical lasers operating in the infrared region, in particular with emission wavelengths falling in the C- and L-bands.

The suitability of fluoride glasses as rare-earth host materials has been known for some time [14] due to their low phonon energies which determine multiphonon relaxation rates and, subsequently, the efficiency of any upconversion processes present. In this paper, we report on a number of upconversion processes identified in an erbium-doped fluoride glass (Er^{3+}:ZBLALiP) microsphere, using a 980 nm pump laser coupled via a fibre taper. Preliminary work on Er^{3+}:ZBLALiP was presented in [7], including evidence of 1550 nm lasing in 1480 nm pumped microspheres. In this paper, we provide a more systematic study of the upconversion processes involved in 980 nm pumping of Er^{3+}:ZBLALiP microspheres. We identify the

[a] e-mail: s.nicchormaic@ucc.ie

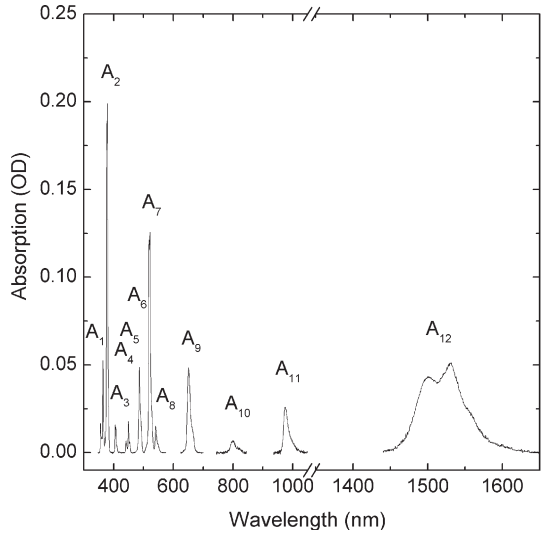

Fig. 1. Absorption spectrum of 0.2 mol% Er^{3+}:ZBLALiP bulk glass.

transitions involved and analyse the dominant processes that give rise to the observed emissions. In addition, we calculate associated material properties through McCumber and Judd-Ofelt theories. We have observed upconversion emissions from the ultraviolet to the infrared and we identify several new emissions including the first observation of a 320 nm upconversion following 980 nm pumping of Er^{3+}. This arises due to the exceptionally long lifetimes of the $^4F_{3,5/2}$ levels within Er^{3+}:ZBLALiP compared to other glasses [15]. The identification and analysis of the numerous upconversions enable us to attribute the emissions to particular erbium transitions and suggest the processes responsible. In addition, the efficiency of the ultraviolet upconversion processes and the stability of erbium doped ZBLALiP microspheres (permitting high optical quality to be achieved during fabrication) make this material suitable for information storage applications where short wavelengths are desirable [16].

2 Experiment

An initial study of some fundamental material properties of Er^{3+} doped ZBLALiP (ZrF_4-BaF_2-LaF_3-AlF_3-LiF-PbF_2) glass was reported earlier [7], where the improved stability of ZBLALiP with respect to similar fluorozirconate glasses and its suitability as a host for rare-earth ions was discussed. Here, we present additional material properties and extend the range of functionality of Er^{3+}:ZBLALiP as a material suitable for optical communications and optical sensing. Figure 1 shows the measured absorption spectrum for a 5.8 mm thick bulk sample of 0.2 mol% Er^{3+}:ZBLALiP in which twelve absorption bands can be identified. These represent the transitions from the ground state $^4I_{15/2} \rightarrow A_N$ with $A_1 = {}^2G_{9/2} + {}^2K_{15/2} + {}^2G_{7/2}$, $A_2 = {}^4G_{11/2}$, $A_3 = {}^2H_{9/2}$, $A_4 = {}^4F_{3/2}$, $A_5 = {}^4F_{5/2}$, $A_6 = {}^4F_{7/2}$, $A_7 = {}^2H_{11/2}$, $A_8 = {}^4S_{3/2}$, $A_9 = {}^4F_{9/2}$, $A_{10} = {}^4I_{9/2}$, $A_{11} = {}^4I_{11/2}$ and $A_{12} = {}^4I_{13/2}$.

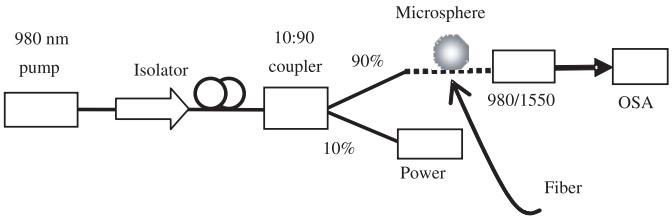

Fig. 2. Experimental setup. OSA – optical spectrum analyser.

The absorption spectra were recorded using a double-beam Cary 17 spectrometer (Varian) with a resolution better than 0.1 nm.

The fabrication techniques for the Er^{3+}:ZBLALiP microspheres was described elsewhere [17]. We use glass with an erbium concentration of 0.2 mol%, which equates to 4×10^{19} Er^{3+} ions/cm^3. Note that, at this concentration, energy transfer (ET) should not play a major role in the upconversion processes and, therefore, excited state absorption (ESA) is the dominant mechanism [18]. Nevertheless, due to the non-trivial problem of distinguishing the two mechanisms, some authors have suggested that ET may play a role even when the dopant concentration is below the critical value of about 1 mol% [19–21].

In our work, the C-band lasing characteristics and upconversion spectra are investigated at room temperature using a single mode, 980 nm laser diode pump with a spectral width of about 1 nm and under CW pumping conditions. The experimental setup is depicted in Figure 2. A fibre-optical isolator is placed immediately after the 980 nm pump laser in order to avoid optical feedback. The pump light then passes through a 10:90 coupler, whereby 10% is monitored using a power meter and the larger fraction is sent through a fibre taper and coupled into the microsphere via evanescent wave coupling. The 980 nm light transmitted through the fibre taper is separated from the C-band emissions using a WDM and an optical spectrum analyser is used to detect the lasing around 1550 nm. The UV to IR emissions are detected by free-space coupling of the scattered radiation from the microsphere into an optical spectrometer. To achieve efficient coupling of the pump into the microsphere and efficient collection of the infrared lasing spectrum, the fibre taper is manufactured using 1550 nm SMF-28 fibre that is adiabatically tapered to 1 μm diameter using a direct heating technique [22]. The transmission loss of these tapers is typically less than 0.1 dB/cm. Optimum mechanical alignment of the taper and microsphere is achieved by translating the microsphere to different locations along the taper until the lasing about 1550 nm is maximized. The transmission through the pump fibre is also monitored during the alignment and around 10–15% of the pump light is coupled into the microsphere. This relatively low coupling efficiency is, in part, due to the broad spectral nature of the pump laser relative to the whispering gallery mode resonances of the microsphere and can be improved by the use of a narrow linewidth pump source [23].

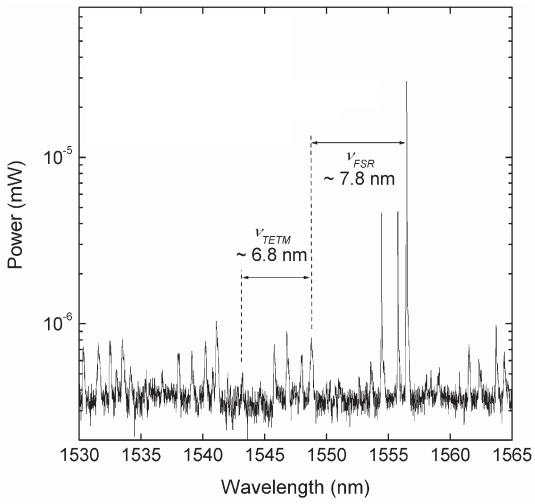

Fig. 3. 70 μm diameter microsphere lasing spectrum (intense peaks) about 1550 nm showing whispering gallery mode structure.

3 Results

Figure 3 shows a typical lasing spectrum obtained for a 70 μm sphere pumped under the aforementioned conditions. Characteristic whispering gallery mode bands about the sphere equator are also observed. The intense peaks represent multimode lasing and the smaller signals indicate fluorescence emissions. The microsphere eccentricity is determined from $\varepsilon = (\Delta\omega_{ecc}/\omega_{nml})\left(l^2/|m| - 1/2\right)$, where l and m are the angular mode numbers, ω_{nml} is the angular frequency of the mode and $\Delta\omega_{ecc}$ is the azimuthal mode splitting. The eccentricity is calculated to be ~2.1% for $l = |m|$ with corresponding azimuthal mode splitting, $\Delta\omega_{ecc}$, of ~11 GHz. Analysis of the lasing peaks enables us to measure the free spectral range, ν_{FSR}, between successive mode groups with a difference in angular mode number l of 1, to be ~7.8 nm (0.97 THz). Theoretically, we can determine the diameter of the sphere from $D = c/\pi p\nu_{FSR}$, where c is the speed of light and p is the refractive index of the material. Using $p = 1.49$ at 1550 nm, we find that $\nu_{FSR} = 7.8$ nm indicates a microsphere diameter of 66 μm, which is reasonably close to the (70 $\pm$ 2) μm determined using an optical microscope.

It can be seen from Figure 3 that each group of modes contains four distinct lasing peaks due to the excitation of multiple modes in the sphere. The peak power of the lasing peaks presented here is ~30 nW, although we have also observed lasing in a single mode with a peak value of ~500 nW. The spacing between TE and TM modes (ν_{TETM}) of 6.8 nm in Figure 3 agrees well with the calculated value of 6.4 nm. An estimate of the loaded cavity Q for this system yields a value in the region of 1×10^7.

The Er^{3+}:ZBLALiP upconversion spectrum recorded coincidently to the C-band lasing spectrum (cf. Fig. 3) is shown in Figure 4. Approximately 700 μW of 980 nm pump light was coupled into the microsphere. The spectrum is detected by monitoring the free-space scattering from the microsphere into a high numerical aperture fibre coupled spectrometer (Ocean Optics USB2000). Due to the limited dynamic linear range of the spectrometer the fluorescence spectrum is produced by splicing two separate spectra together. This also enables us to maximize the signal-to-noise ratio of the lower intensity transitions. The spectra about the green were recorded for a detector integration time reduced by a factor of 40. Thirteen discrete peaks have been noted in the spectrum and are numbered from T1–T13. The spectra have also been corrected for the responsivity of the spectrometer detector as a function of wavelength. The total power outcoupled and detected is 0.5 nW for the green transitions (T6 and T7) and 0.1 nW for T13. The limited resolution of the spectrometer used, combined with the smaller microsphere free spectral range at shorter wavelengths, means that the whispering gallery mode structure is only visible for emissions at wavelengths above 800 nm. The mode structure for the 849 nm (T13) emission is distinguishable in the inset of Figure 4.

3.1 Emission and absorption cross-sections of Er^{3+}:ZBLALiP

The emission cross-section, σ_{ems}, for Er^{3+}:ZBLALiP around 1550 nm can be determined from the absorption spectrum (Fig. 1). Using McCumber theory, under the assumption of a strongly phonon coupled system [24], the emission cross-section is given by

$$\sigma_{ems}(\lambda) = \sigma_{abs}(\lambda)\frac{Z_L}{Z_U}\exp\left(\frac{E_{UL}}{k_BT}\right)\exp\left(-\frac{hc}{\lambda k_BT}\right), \quad (1)$$

where Z_L (Z_U) is the partition function of the lower (upper) state given by a summation of continuous levels $\sum_i \exp(\Delta E_i/k_BT)$, where ΔE_i is the energy difference between the Stark split sublevels and the lowest energy level in the lower (upper) manifold, E_{UL} is the energy difference between the lowest sublevels in the upper and lower manifolds, h is Planck's constant, c is the speed of light, k_B is Boltzmann's constant, and T is temperature in Kelvin. From equation (1), the bulk sample of Er^{3+}:ZBLALiP has a peak emission cross-section of 4.6×10^{-21} cm^2 in the C-band, which compares well with values of 4.9×10^{-21} cm^2 measured for fluoroindate glasses [15] and 4.6×10^{-21} cm^2 measured in other fluorozirconate glass bulk samples [25].

Using the absorption data presented in Figure 1, it is also possible to determine the absorption cross-section using the expression [20]

$$\sigma_{abs} = \frac{-\log A}{l\,N'} \quad (2)$$

where A is the absorbance, l is the sample thickness, and N' is the Er^{3+} concentration of 3.76×10^{19} cm^{-3}. Figure 5 presents the absorption and emission cross-sections for 0.2 mol% Er^{3+}:ZBLALiP in the C-band. Emission spectra for both bulk and powder ZBLALiP samples are shown.

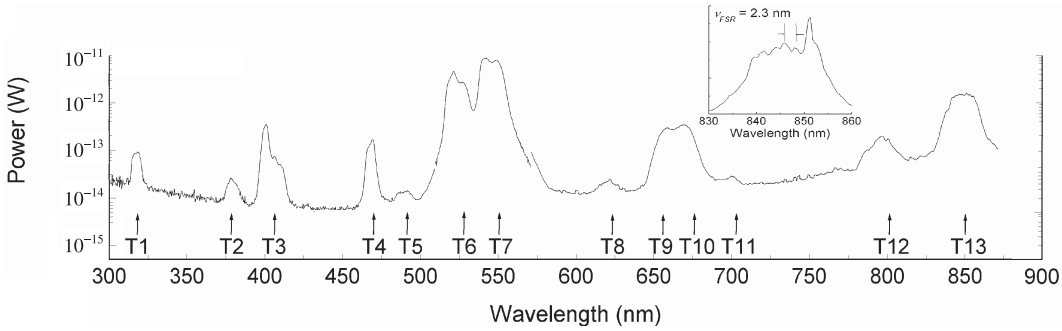

Fig. 4. Er^{3+}:ZBLALiP microsphere upconversion spectrum. The spectrometer integration time was reduced by a factor of forty about the green transitions T6 and T7. Inset: whispering gallery mode structure about T13.

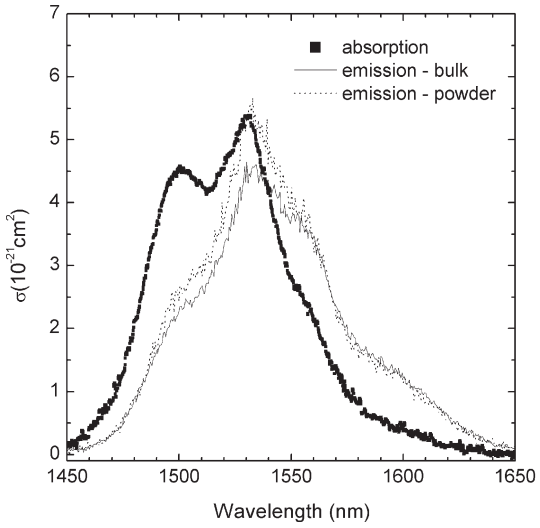

Fig. 5. Absorption (bulk) and emission (bulk and powder) cross-section measurements for 0.2 mol% Er^{3+}:ZBLALiP.

3.2 Radiative properties of Er^{3+}:ZBLALiP

In order to gain a thorough understanding of the emission processes within Er^{3+}:ZBLALiP its radiative properties can be determined through Judd-Ofelt (JO) analysis of the absorption data presented in Figure 1. The JO intensity parameters Ω_t (t = 2, 4, 6) are derived from the electric-dipole contributions of the measured line strengths by a least-squares-fitting approach to minimize the root mean square deviation with the calculated line strength. Values of $\Omega_2 = 3.12 \times 10^{-20}$ cm^2, $\Omega_4 = 1.49 \times 10^{-20}$ cm^2, and $\Omega_6 = 1.15 \times 10^{-20}$ cm^2 [7] are used throughout our calculations. A spectroscopic quality factor can be defined as Ω_4/Ω_6, which gives 1.30 for the quoted intensity parameters. Note that the JO parameters for Er^{3+}:ZBLALiP are slightly higher than those for Er^{3+}:ZBLAN ($\Omega_2 = 2.37 \times 10^{-20}$ cm^2, $\Omega_4 = 1.24 \times 10^{-20}$ cm^2, and $\Omega_6 = 0.73 \times 10^{-20}$ cm^2) [26]. A higher Ω_2 indicates greater asymmetry of the host glass, while a higher Ω_6 has a dominant influence on the electric dipole line strength, S^{ed}, of the lasing transition $^4I_{13/2} \rightarrow {}^4I_{15/2}$ [27].

Determination of the electric dipole line strength, S^{ed}, and the magnetic dipole line strength, S^{md}, combined with the JO intensity parameters for our material, can be used to predict significant radiative properties for Er^{3+}:ZBLALiP such as the spontaneous radiative transition rates, electric dipole line strengths, branching ratios and radiative lifetimes. S^{ed} depends on the double reduced matrix elements of the unit tensor operator, U, and these are assumed to be independent of the host material [27]. Following this argument we have taken average published matrix elements [27,28] for our calculations and these are reproduced in Table 1 for convenience. S^{md} depends on the double reduced matrix elements of the $L + 2S$ operator, where L is the total orbital angular momentum and S is the total spin.

The total spontaneous radiative transition rate between two levels J and J', is given by

$$A_{JJ'} = A^{ed}_{JJ'} + A^{md}_{JJ'} = \frac{64\pi^4}{3h\lambda^3(2J+1)} \left(\chi_{ed} S^{ed} + \chi_{md} S^{md}\right), \quad (3)$$

where λ is the mean wavelength of the absorption, $\chi_{ed} = p(p^2+2)^2/9$ is the local field correction factor for electric dipole transitions, and $\chi_{md} = p^3$ is the local field correction factor for magnetic dipole transitions. We calculate the magnetic dipole emission probabilities, $A^{md}_{JJ'}$, using published values [27] for LaF_3 ($A'^{md}_{JJ'}$) and corrected for the refractive index difference using the relation $A^{md}_{JJ'} = (p/p')^3 A^{md}_{JJ'}$, where p' (p) is the refractive index of LaF_3 (ZBLALiP). The refractive index for ZBLALiP is 1.49 at 1550 nm, while that for LaF_3 is 1.57, hence $A^{md}_{JJ'} = 0.86 A'^{md}_{JJ'}$.

The radiative lifetime, τ_R, of transitions between levels J and J' is related to the inverse of $A_{JJ'}$ by

$$\tau_R = \frac{1}{\sum_{J'} A_{JJ'}}, \quad (4)$$

and the branching ratio, β, between J and J' is simply the ratio of $A_{JJ'}$ for the initial level to the sum of $A_{JJ'}$ for all the lower levels given by

$$\beta = A_{JJ'} \tau_R. \quad (5)$$

Table 1 shows our values for the radiative probabilities, electric dipole line strengths, branching ratios, and

radiative lifetimes for the transitions involved in 980 nm pumped Er^{3+}:ZBLALiP. Several levels have high branching ratios for transitions to the ground level and intermediate levels, many of which have been observed in the emission spectrum in Figure 4. Where possible we have identified the transition associated with the emissions observed in Figure 3 and have indicated this correspondence in the average wavelength column. Note that the radiative properties for the observed 667 nm emission (T10) have not been calculated due to limited data availability and, therefore, it does not appear in Table 1.

4 Discussions

In Figure 6 we present an energy level diagram for erbium indicating the radiative and non-radiative transitions that are responsible for the thirteen emissions identified in Figure 4. Even though it is energetically possible for several emissions to originate from the same level, the branching ratios, β, predicted in the JO theory can help determine the most likely emissions from a particular level. For example, it is energetically possible for both the 383 nm (T2) and 618 nm (T8) emissions to originate from the radiative decay of $^4G_{11/2}$ to lower levels. However, the ratio of the measured emission intensities (1:3) disagrees substantially from the calculated ratios (1:21), thereby indicating that both emissions cannot arise from the $^4G_{11/2}$ level. In fact, only the 383 nm emission is from $^4G_{11/2}$ and the 618 nm emission is due to the $^2P_{3/2} \rightarrow {}^4F_{9/2}$ decay. In this way, we can use a combination of the energy gaps between the energy levels and the calculated branching ratios to determine the energy levels involved in the radiative emissions.

Four emissions in Figure 4 are attributed to the decay of the $^2P_{3/2}$ level. These are the 618 nm (T8) decay to $^4F_{9/2}$ ($\beta = 0.05$), the 479 nm (T4) decay to $^4I_{11/2}$ ($\beta = 0.29$), the 403 nm (T3) decay to $^4I_{13/2}$ ($\beta = 0.39$), and the 320 nm (T1) decay to $^4I_{15/2}$ ($\beta = 0.12$). The branching ratio calculations predict the ratio of emission intensities for each of the levels to be 1 (618 nm):5.8 (470 nm):7.8 (403 nm), which is in reasonable agreement with the measured ratios of 1:5.3:6.6. We have excluded the intensity of the 320 nm emission from this comparison because fluorozirconate glasses have very substantial absorption losses in the UV region [29].

Further understanding of the transition(s) responsible for a particular wavelength can be obtained by the intensity dependence behaviour of the fluorescence at a particular wavelength. The centre wavelength associated with each transition is also shown in Figure 6. In the case of ESA, the dependence of the fluorescence intensity upon pump power often exhibits a simple power law dependence with a slope, n, equal to the number of photons absorbed. Measurements of this dependence for the case of the observed green transitions $^2H_{11/2} \rightarrow {}^4I_{15/2}$ (T6) and $^4S_{3/2} \rightarrow {}^4I_{15/2}$ (T7) are presented in Figure 7, where we plot the intensity as a function of the absorbed pump power in the fibre taper. From the energy diagram (cf. Fig. 6) both T6 and T7 are attributed to 2-photon absorption. Slopes corresponding to $n = 1.58$ for T6 and $n = 1.66$ for T7 have been recorded, whereas a slope of two would be expected. This discrepancy from the expected result can be understood as depletion of the $^4I_{15/2}$ ground state [9].

Based on our analysis we predict that the $^4F_{3,5/2}$ levels of Er^{3+}:ZBLALiP have unusually long radiative lifetimes of 1.44 ms and 1.15 ms compared to other glasses, such as Er^{3+}-doped fluoroindate glass which has a lifetime of 0.50 ms [15]. As can be seen from the energy level diagram (cf. Fig. 6), this is critically important for the generation and observation of UV and violet emissions from the $^2P_{3/2}$ level since it facilitates the third ESA, $^4F_{3,5/2} \rightarrow {}^2K_{13/2}$, by maintaining a large $^4F_{3,5/2}$ population. In Er^{3+}-doped fluoroindate glass, nonradiative decay rapidly depletes the $^4F_{3,5/2}$ population, effectively preventing any further ESA and prohibiting UV emissions.

Our measurements demonstrate a broad range of emission from 320 nm to 849 nm in Er^{3+}:ZBLALiP, in addition to the IR lasing around 1550 nm. We suggest that the combination of high cavity quality factor and low whispering gallery mode volume (approximately 2000 μm^3) significantly enhances the probability of excited state absorption by enhancing the pump field strength ($\sim 10^3$ V/m per photon) within the microsphere. This is reflected in the fact that a significant number of the observed transitions are attributed to 3-photon and 4-photon absorption events for what is a relatively modest pump power (sub mW) coupled into the microsphere.

The emission line centred at 320 nm (T1) is, most likely, due to a 4-photon process populating the $^2P_{3/2}$ state, which in turn radiatively relaxes to the $^4I_{15/2}$ ground state. Three pump photons populate the $^2G_{7/2}$ state. The $^2G_{7/2}$–$^2P_{3/2}$ energy gap of $\sim$3600 cm^{-1} combined with a phonon energy of 650 cm^{-1} is such that the $^2P_{3/2}$ state is unlikely to be populated by thermalisation and, as such, we suggest that the absorption of a fourth pump photon is necessary to explain T1. This 320 nm transition has previously been reported in Er^{3+}-doped glass, but was identified as a 3-photon process following pumping at 637 nm [16]. The same authors also reported emissions corresponding to the transitions T3, T4, T7 and T9. Transition T1 has been reported [30] in an Yb^{3+}:Er^{3+} co-doped material although in that case the excitation process involved successive energy transfers from Yb^{3+}. It should be noted that this is very different from our work which involves a single dopant i.e. erbium and, therefore, does not rely on a sensitizer ion. Additionally, ETU does not play a major role in our experiments due to the low dopant concentration.

We believe that the transitions $^2P_{3/2} \rightarrow {}^4I_{13/2}$ (T3), $^2P_{3/2} \rightarrow {}^4I_{11/2}$ (T4) and $^2P_{3/2} \rightarrow {}^4F_{9/2}$ (T8) also arise due to 4-photon excitation. Transitions T1, T3 and T4 have been observed following pumping at 545 nm [31]. Transitions T6, T7, T12 and T13 have been reported following 980 nm pumping [32]. The ultraviolet line

Table 1. Predicted radiative transition probabilities electric dipole line strengths (S^{ed}) ($A^{ed}_{JJ'}$and$A^{md}_{JJ'}$), branching ratios (β), and radiative lifetimes (τ_R) for Er^{3+}:ZBLALiP. Note that the number in brackets (T1, T2, ...) listed under the average wavelength corresponds to the observed transitions in Figure 3.

Transition	Average wavelength (nm)	$\left[U^{(2)}\right]^2$	$\left[U^{(4)}\right]^2$	$\left[U^{(6)}\right]^2$	S^{ed} ($\times 10^{-20}$cm^3)	$A^{ed}_{JJ'}$ (s^{-1})	$A^{md}_{JJ'}$ (s^{-1})	β	τ_R (ms)
$^4I_{13/2} \rightarrow$ $^4I_{15/2}$	1542	0.0195	0.1173	1.4316	1.88	78	32.2	1.00	9.10
$^4I_{11/2} \rightarrow$ $^4I_{15/2}$	975	0.0282	0.0003	0.3953	0.54	98	7.2	0.84	8.53
$\rightarrow$ $^4I_{13/2}$	2727	0.0210	0.1100	1.0400	1.43	12		0.16	
$^4I_{9/2} \rightarrow$ $^4I_{15/2}$	793 (T12)	0.0000	0.1733	0.0099	0.27	106	1.0	0.76	7.14
$\rightarrow$ $^4I_{13/2}$	1668	0.0003	0.0081	0.6400	0.75	32		0.23	
$\rightarrow$ $^4I_{11/2}$	4663	0.0030	0.0674	0.1271	0.26	1		0.01	
$^4F_{9/2} \rightarrow$ $^4I_{15/2}$	656 (T9)	0.0000	0.5354	0.4618	1.33	947	5.1	0.89	0.938
$\rightarrow$ $^4I_{13/2}$	1025	0.0096	0.1576	0.0870	0.36	67	2.2	0.06	
$\rightarrow$ $^4I_{11/2}$	1966	0.0671	0.0088	1.2611	1.67	44		0.05	
$\rightarrow$ $^4I_{9/2}$	3623	0.0960	0.0061	0.0120	0.32	1		0.00	
$^4S_{3/2} \rightarrow$ $^4I_{15/2}$	540 (T7)	0.0000	0.0000	0.2211	0.25	700		0.66	0.949
$\rightarrow$ $^4I_{13/2}$	849 (T13)	0.0000	0.0000	0.3481	0.40	294		0.28	
$\rightarrow$ $^4I_{11/2}$	1212	0.0000	0.0037	0.0789	0.10	24		0.02	
$\rightarrow$ $^4I_{9/2}$	1688	0.0000	0.0729	0.2560	0.40	36		0.03	
$^2H_{11/2} \rightarrow$ $^4I_{15/2}$	520 (T6)	0.7056	0.4109	0.0870	2.91	3453	54.5	0.92	0.265
$\rightarrow$ $^4I_{13/2}$	792	0.0230	0.0611	0.0527	0.22	75	81.5	0.03	
$\rightarrow$ $^4I_{11/2}$	1115	0.0357	0.1382	0.0371	0.36	43	0	0.03	
$\rightarrow$ $^4I_{9/2}$	1507	0.2077	0.0662	0.2858	1.08	53	0.2	0.01	
$\rightarrow$ $^4F_{9/2}$	2579	0.3629	0.0224	0.0022	1.17	11		0.00	
$^4F_{7/2} \rightarrow$ $^4I_{15/2}$	492 (T5)	0.0000	0.1467	0.6273	0.94	1964		0.78	0.397
$\rightarrow$ $^4I_{13/2}$	727	0.0000	0.3371	0.0001	0.50	316		0.13	
$\rightarrow$ $^4I_{11/2}$	983	0.0035	0.2648	0.1515	0.58	147		0.06	
$\rightarrow$ $^4I_{9/2}$	1245	0.0163	0.0954	0.4277	0.68	86		0.03	
$\rightarrow$ $^4F_{9/2}$	1947	0.0121	0.0342	0.0151	0.11	4		0.00	
$^4F_{5/2} \rightarrow$ $^4I_{15/2}$	450	0.0000	0.0000	0.2237	0.26	873		1.00	1.15
$^4F_{3/2} \rightarrow$ $^4I_{15/2}$	443	0.0000	0.0000	0.1204	0.14	690		1.00	1.44
$^2H_{9/2} \rightarrow$ $^4I_{15/2}$	409	0.0000	0.0190	0.2255	0.29	831	31.1	0.33	0.400
$\rightarrow$ $^4I_{13/2}$	556	0.0780	0.1194	0.3535	0.83	953	0.9	0.38	
$\rightarrow$ $^4I_{11/2}$	697 (T11)	0.0428	0.0824	0.1128	0.39	226	36.5	0.10	
$\rightarrow$ $^4I_{9/2}$	823	0.0147	0.0062	0.0043	0.06	21	0.9	0.01	
$\rightarrow$ $^4F_{9/2}$	1079	0.0055	0.0314	0.0369	0.11	184	0.7	0.09	
$\rightarrow$ $^2H_{11/2}$	1854	0.0308	0.1828	0.0671	0.45	152		0.06	
$\rightarrow$ $^4F_{7/2}$	2485	0.1058	0.0488	0.0240	0.43	61		0.02	
$^4G_{11/2} \rightarrow$ $^4I_{15/2}$	383 (T2)	0.9178	0.5271	0.1197	3.79	11620	37.9	0.84	0.072
$\rightarrow$ $^4I_{13/2}$	505	0.1011	0.2642	0.2550	1.00	1300	0.1	0.10	
$\rightarrow$ $^4I_{11/2}$	618	0.0002	0.4930	0.0144	0.75	527	0.6	0.04	
$\rightarrow$ $^4I_{9/2}$	724	0.0645	0.0117	0.0467	0.27	120	2.6	0.01	
$\rightarrow$ $^4F_{9/2}$	905	0.4436	0.0388	0.0104	1.45	328	10.2	0.02	
$\rightarrow$ $^2H_{11/2}$	1394	0.0006	0.1600	0.1100	0.37			0.00	
$^4G_{9/2} \rightarrow$ $^4I_{15/2}$	365	0.0000	0.2416	0.1235	0.50	2034		1.00	0.492
$^2G_{7/2} \rightarrow$ $^4I_{15/2}$	358	0.0000	0.0174	0.1163	0.16	839		1.00	1.192
$^2P_{3/2} \rightarrow$ $^4I_{15/2}$	320 (T1)	0.0000	0.0000	0.0260	0.03	403	19.5	0.12	0.310
$\rightarrow$ $^4I_{13/2}$	403 (T3)	0.0000	0.0000	0.1600	0.18	1242		0.39	
$\rightarrow$ $^4I_{11/2}$	470 (T4)	0.0000	0.1300	0.0250	0.22	936		0.29	
$\rightarrow$ $^4I_{9/2}$	524	0.0000	0.0440	0.0092	0.08	230		0.07	
$\rightarrow$ $^4F_{9/2}$	618 (T8)	0.0000	0.0560	0.0045	0.09	164		0.05	
$\rightarrow$ $^4S_{3/2}$	763	0.0847	0.0000	0.0000	0.26	259		0.09	
$^2K_{13/2} \rightarrow$ $^4I_{15/2}$	302	0.0032	0.0029	0.0152	0.03	167		1.00	5.99

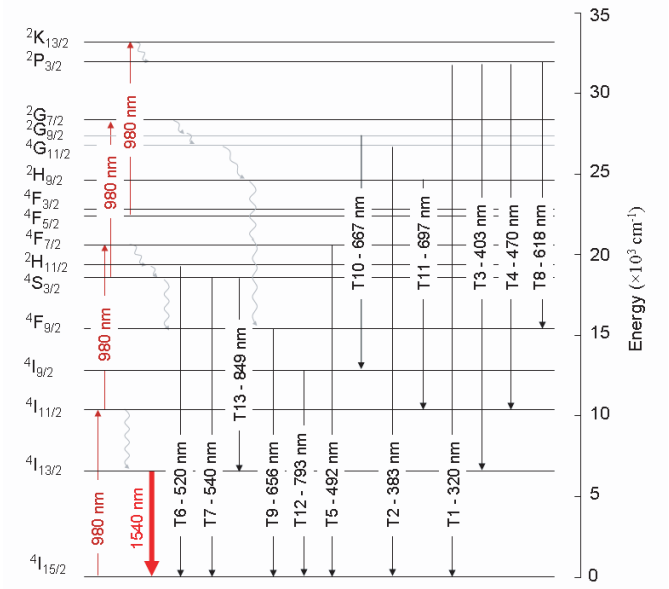

Fig. 6. Erbium energy level diagram with radiative (solid lines) and non-radiative transitions. The thick, red line at 1540 nm indicates the C-band lasing transition.

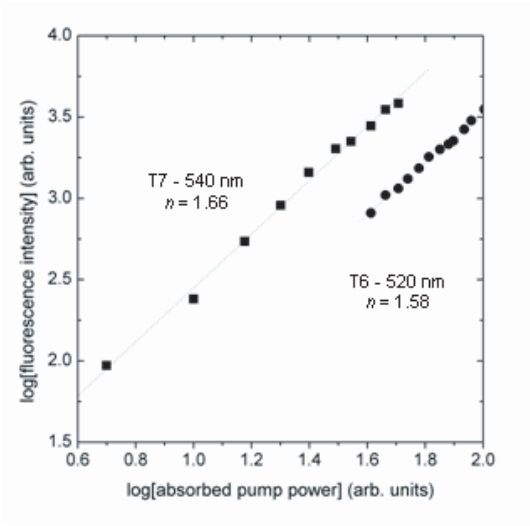

Fig. 7. Intensity dependence of 70 μm diameter Er^{3+}:ZBLALiP microsphere green emissions T6 and T7.

at 383 nm (T2) and the 492 nm emission (T5) have been reported under 973 nm excitation [33].

Notably, we have also observed emissions about 700 nm (T11). Previous Er^{3+} emission at 700 nm has been attributed to the transition $^4F_{7/2} \rightarrow {}^4I_{13/2}$ following absorption of three pump photons at 1480 nm [34]. This seems unlikely in our case, since the JO theory suggests that a 492 nm emission would be more probable than a 700 nm emission from $^4F_{7/2}$. We presume this assignment was on the basis of the 3-photon resonance $^4F_{7/2} \rightarrow {}^4I_{15/2}$. As an alternative, we propose this emission follows the transition $^2H_{9/2} \rightarrow {}^4I_{11/2}$, which is in better agreement with the energy gap between the levels and the JO theory. Finally, we have observed emissions centred at 618 nm (T8) and 667 nm (T10) that have not been observed elsewhere for 980 nm pumping of Er.

5 Conclusions

In conclusion, we have demonstrated a multiwavelength microsphere light source for microphotonic applications [35] fabricated using Er^{3+}:ZBLALiP and we have identified the Er^{3+} transitions involved in the material through a combination of Judd-Ofelt analysis, the erbium energy level diagram and the published centre wavelengths. Upconversion emissions from 320 nm to 849 nm and 1550 nm lasing have been observed. We propose that a number of the upconversion transitions are attributable to 3- and 4-photon processes, in contrast to previous observations for erbium-doped glasses. This is due to the long erbium lifetimes within Er^{3+}:ZBLALiP that favour higher order photon absorptions and, consequently, emissions in the UV at 320 nm have been observed. These results indicate that Er^{3+}:ZBLALiP is an attractive alternative to Er^{3+}:ZBLAN for information-storage applications where even very small powers are sufficient for data retrieval operations [16] and its improved stability [7] promises easier fabrication of devices using ZBLALiP such as erbium doped fibres, microspheres and optical switches. Future work will focus on using integrated optics for the device based on waveguide technology [36] that will enable us to improve the detection efficiency for the upconversion spectrum.

This work is funded by Science Foundation Ireland under grant 02/IN1/128. D. O'Shea acknowledges generous support from IRCSET through the Embark Initiative.

References

1. L. Collot, V. Lefèvre-Sequin, M. Brune, J.M. Raimond, S. Haroche, Europhys. Lett. **23**, 327 (1993)
2. H. Mabuchi, H.J. Kimble, Opt. Lett. **19**, 749 (1994)
3. W. von Klitzing, E. Jahier, R. Long, F. Lissillour, V. Lefèvre-Seguin, J. Hare, J.-M. Raimond, S. Haroche, J. Opt. B **2**, 204 (2000)
4. M. Cai, G. Hunziker, K.J. Vahala, IEEE Photon. Technol. Lett. **6**, 686 (1999)
5. T. Bilici, S. Isci, A. Kurt, A. Serpengüzel, IEEE Photon. Technol. Lett. **16**, 476 (2004)
6. F. Lissillour, D. Messager, G. Stéphan G.P. Féron, Opt. Lett. **26**, 1051 (2001)
7. M. Mortier, P. Goldner, P. Féron, G.M. Stephan, H. Xu, Z. Cai, J. Non-Cryst. Sol. **326**, **327**, 505 (2003)
8. M.-F. Joubert, Opt. Mat. **11**, 181 (1999)
9. H. Fujiwara H.K. Sasaki, J. Appl. Phys. **86**, 2385 (1999)
10. H. Fujiwara, K. Sasaki, Jpn J. Appl. Phys. **41**, L46 (2002)
11. M. Cai, O. Painter, K.J. Vahala, Opt. Lett. **25**, 1430 (2000)
12. X. Peng, F. Song, S. Jiang, N. Peyghambarian, M. Kuwata-Gonokami, L. Xu, Appl. Phys. Lett. **82**, 1497 (2003)
13. J. Wu, S. Jiang, T. Qua, M. Kuwata-Gonokami, N. Peyghambarian, Appl. Phys. Lett. **87**, 211118 (2005)

14. D.S. Funk, J.G. Eden, IEEE J. Sel. Top. Quant. Elec. **1**, 784 (1995)
15. A. Florez, Y. Messaddeq, O.L. Malta, M.A. Aegerter, J. Alloys Comp. **227**, 135 (1995)
16. C.L. Pope, B.R. Reddy, S.K. Nash-Stevenson, Opt. Lett. **22**, 295 (1997)
17. F. Lissilour, P. Féron, N. Dubreuil, P. Dupriez, G.M. Stéphan, M. Poulain, Proc. SPIE **3611**, 199 (1999)
18. J.P. van der Ziel, F.W. Ostermayer, L.G. van Uitert, Phys. Rev. B **2**, 4432 (1970)
19. R. Rolli, M. Montagna, A. Chiasera, G.C. Righini, S. Pelli, A. Jha, V.K. Tikhomirov, S.A. Tikhomirova, A. Monteil, S. Chaussedent, M. Ferrari, Phil. Mag. B **82**, 573 (2002)
20. T. Catunda, L.A.O. Nunes, A. Florez, Y. Messaddeq, M.A. Aegerter, Phys. Rev. B **53**, 6065 (1996)
21. M.D. Shinn, W.A. Sibley, M.G. Drexhage, R.N. Brown, Phys. Rev. B **27**, 6635 (1983)
22. J.M. Ward, D.G. O'Shea, B.J. Shortt, M.J. Morrissey, K. Deasy, S.G. Nic Chormaic, Rev. Sci. Instrum. **77**, 083105 (2006)
23. J.C. Knight, G. Cheung, F. Jacques, T.A. Birks, Opt. Lett. **22**, 1129 (1997)
24. C. Florea, K.A. Winick, J. Lightwave, Technol. **17**, 1593 (1999)
25. R.M. Martin, R.S. Quimby, J. Opt. Soc. B **23**, 1770 (2006)
26. S.R. Bullock, B.R. Reddy, P. Venkateswarlu, S.K. Nash-Stevenson, J.C. Fajardo, Opt. Quant. Electron. **29**, 83 (1997)
27. M.J. Weber, Phys. Rev. **157**, 262 (1967)
28. W.T. Carnall, P.R. Fields, K. Rajnak, J. Chem. Phys. **49**, 4424 (1968)
29. P.W. France, M.G. Drexhage, J.M. Parker, M.W. Moore, S.F. Carter, J.V. Wright, *Fluoride Glass Optical Fibres* (CRC Press Inc., Florida, 1990)
30. L.F. Johnson, J.E. Geusic, H.J. Guggenheim, T. Kushida, S. Singh, L.G. van Uitert, Appl. Phys. Lett. **15**, 48 (1969)
31. H. Xu, Z. Jiang, Phys. Rev. B **66**, 035103-1 (2002)
32. F. Vetrone, J.-C. Boyer, J.A. Capobianco, A. Speghini, M. Bettinelli, Appl. Phys. Lett. **80**, 1752 (2002)
33. A. Biswas, G.S. Maciel, C.S. Friend, P.N. Prasad, J. Non-Cryst. Sol. **316**, 393 (2003)
34. S. Arahira, K. Watanabe, K. Shinozaki K.Y. Ogawa, Opt. Lett. **17**, 1679 (1992)
35. B.E. Little, J.-P. Laine, D.R. Lim, H.A. Haus, Opt. Lett. **25**, 73 (2000)
36. S. Kobayashi, Proc. SPIE **2997**, 264 (1997)